A model for many-body interaction effects in open quantum dot systems

2003 J. Phys.: Condens. Matter 15 147

(http://iopscience.iop.org/0953-8984/15/2/314)

INSTITUTE OF PHYSICS PUBLISHING JOURNAL OF PHYSICS: CONDENSED MATTER

J. Phys.: Condens. Matter **15** (2003) 147–158 PII: S0953-8984(03)54206-0

A model for many-body interaction effects in open quantum dot systems

K M Indlekofer[1], J P Bird, R Akis, D K Ferry and S M Goodnick

Department of Electrical Engineering and Center for Solid State Electronics Research, Arizona State University, Tempe, AZ 85287-5706, USA

Received 2 October 2002
Published 20 December 2002
Online at stacks.iop.org/JPhysCM/15/147

Abstract

We discuss the influence of the electron–electron interaction on transport properties of open quantum dot systems. Based on the idea of the Anderson model, we present interaction-induced temperature-dependent corrections to the conductance beyond the single-particle picture.

1. Introduction

In contrast to a quantum dot in the tunnelling regime, where the discrete eigenstates of the corresponding closed system give rise to sharp transmission resonances through the system, usually most of these resonances in open dots are broadened out due to a large imaginary part of the coupling self-energy to the leads. Nevertheless, even in the open system, some of the localized resonances are persistent, strongly depending on the geometry of the open system, especially dot shape and lead positions [1–4]. These persistent states tend to correspond to periodic orbits of the classical chaotic system [5, 6]. The projection of the propagating single-particle states of the open dot system onto the discrete eigenstates of the closed system reflects strong resonances at individual, discrete closed-dot states, representing exactly those states of localized charge inside the quantum dot [3, 4]. Recent experimental results [7–11] investigating the temperature dependence of conductance fluctuations in open dots and dot arrays show good agreement with the single-particle theory [1–3, 12] at high temperatures. At lower temperatures however, deviations from the single-particle picture have been observed, with clearly resolved metal-like and insulator-like phases in the conductance maxima and minima, respectively [7–11]. Magneto-transport measurements and results for reference samples without quantum dots clearly rule out weak localization effects of the electron gas as the origin of the deviations [10, 13, 14]. It has been suggested that this finding could be attributed to a confinement-enhanced electron interaction [13]. (One has to note that Coulomb blockade effects of the tunnelling regime are quenched in open dot systems.) Hence, many-body interaction effects [15] analogous to those seen in quantum dots in the tunnelling regime [16–21] might also play an important role in open dot systems.

[1] Current address: ISG, Research Centre Jülich, D-52425 Jülich, Germany.

0953-8984/03/020147+12$30.00

In this paper, we present a many-body model based on the Anderson model [16–22] and the idea of an enhanced electron–electron interaction inside the open quantum dot in the vicinity of a resonant state. This approach is physically based on the charge resonance inside the quantum dot observed in single-particle simulations [3, 4] considering the projection of resonant states to closed quantum dot states.

In the following, we will first present a short discussion of the physics of open quantum dot systems. The next section defines the many-body model interaction Hamiltonian and the non-equilibrium many-body density-matrix approach employed to describe transport through an open system. A subsequent mean-field approach to the model helps to significantly reduce the dimensionality of the problem. We will show numerical simulations for the temperature dependence of the conductance corrections due to the interaction. We find that a characteristic temperature [20, 21, 23] can be defined in the model to characterize two temperature regimes. Furthermore, exchange-enhanced spin polarization is studied.

2. The physics of open quantum dots

In this section, we briefly review some of the previously established features of electron transport in open quantum dots, which will provide the justification for the assumptions that underlie our many-body transport model. It is well understood that the energy of electrons in weakly coupled quantum dots is quantized into a series of discrete energy levels [24]. It is generally less well appreciated, however, that at least some of the states of this spectrum remain resolved in open semiconductor dots, which are coupled to their external reservoirs by means of few-mode quantum point contact leads [1, 2, 25–28]. The key feature here is a *non-uniform* broadening of the eigenstates, which arises when the dot is open via the point contacts. The reason for this non-uniform broadening has been discussed in some detail, but is basically a consequence of quantum mechanical collimation; in order for electrons to enter or leave the dot, they must pass enter the associated point contact at an angle, so that their transverse momentum component matches one of the quantized values associated with the different one-dimensional subbands in the lead [1]. At certain energies, this results in a resonant trapping of Fermi-level electrons in the dot, so that they are only able to escape the dot on a timescale several orders of magnitude longer than the direct transit time across the dot [28]. It is this trapping at specific energies that leads us to assume below a strong enhancement of the effective electron interaction in the dot, at certain energies. In particular, a critical consequence of this trapping is that, *even though the dot is open, electrons are not able to flow freely into, or out of, it*. The signature of this resonant trapping is easily identified in experiment, in which a magnetic field, or a gate voltage variation, may be used to sweep the resolved density of states past the dot, giving rise to oscillations in the conductance [1, 2, 25, 26]. The basic periodicity of these oscillations has previously been successfully interpreted [2, 25] in terms of the presence of strongly scarred wavefunction states, which recur in intensity as the external parameter (magnetic field or gate voltage) is varied. In this paper, however, we wish to consider the many-body implications of this basic transport picture.

3. Interaction model

The Anderson model [16–22] describes the coupling of a single impurity level with an on-site electron–electron interaction to a one-dimensional lead by use of a tight-binding single-particle basis. In our case, the single impurity is interpreted as a quantum dot coupled to two open leads. The impurity level then describes the discrete, closed dot state corresponding to a single

persistent open dot resonance. In order to obtain a numerically tractable many-body Fock space model for the interacting open quantum dot system, we reformulate the Anderson model in the eigenbasis of the coupled dot–lead system without interaction. The choice of this open eigenbasis accounts for the fact that the system is open. These propagating 1D eigenstates $\psi_{nk\sigma}$ (indexed by the point contact wavenumber k, lateral mode number n and spin σ) of the continuous spectrum typically exhibit Fano resonances in the transmission probability. $t_{nk\sigma}$ [29], reflecting resonances of the open dot. Possible eigenstates of the discrete spectrum inside the open quantum dot (i.e. fully bound states in the lower energy region) will not be further discussed here, since we assume that they are always occupied and only contribute to the single-particle potential of the system. In the following, we assume that the dispersion relation $\varepsilon_{nk\sigma}$ and the transmission probability $t_{nk\sigma}$ of the propagating states through the open dot are already known from single-particle simulations [1–3, 12] for the given realistic 3D potential (and the external magnetic field). The many-body interaction part (with the leading Coulomb-matrix elements $V_{(nk\sigma)(n'k'\sigma')}$) in the total Hamiltonian is assumed to be diagonal in Fock space concerning the propagating mode single-particle base. Note that we consider a full many-body state space in this approach. (The chosen interaction Hamiltonian is not fully equivalent to the original tight-binding interaction part of the Anderson Hamiltonian [22, 23] transformed to the new base. However, in contrast to the diagrammatic approach to the Anderson system which considers the coupling between the dot and the reservoirs as a perturbation, we fully account for this coupling by choosing the open eigenbasis.) The crucial step in constructing these interaction matrix elements is based on the physical argument that the on-site repulsion in the tight-binding Anderson model is transformed to an energetically peaked interaction between propagating states in the vicinity of each resonance. Furthermore, we can also justify a peaked interaction in the continuum of propagating states based purely on the existence of resonant states. Considering the projection amplitudes of single-particle states of the open dot onto the discrete closed dot states [3, 4] we see a resonance of charge (i.e., $\int_{dot} |\psi|^2 \, \mathrm{d}^3x$) inside the quantum dot. This means that the resulting interaction matrix elements obviously exhibit a resonance. We therefore want to interpret the peaked interaction term as an excess interaction due to the localization of charge inside the quantum dot with each resonant state. (One has to note that, although the quantum dot is open, we do not deal with Coulomb interaction terms of an unrestricted electron gas. The interaction effects we consider here arise due to a resonantly trapped charge at certain energies, quasi-bound within the quantum dot between two quantum point contacts.) Finally, the effective model Hamiltonian (normalized to $-k_BT$) for the open dot system reads (compare with [30])

$$\hat{H} = -\beta\left[\sum_{n,k,\sigma}(\varepsilon_{nk\sigma} - \mu_k)c^+_{nk\sigma}c_{nk\sigma} + \tfrac{1}{2}\sum_{(nk\sigma)\neq(n'k'\sigma')} V_{(nk\sigma)(n'k'\sigma')}c^+_{nk\sigma}c_{nk\sigma}c^+_{n'k'\sigma'}c_{n'k'\sigma'}\right], \qquad (1)$$

with $\beta = 1/k_BT$, μ_k the chemical potential for wave k and $c_{nk\sigma}$ the annihilation operator. Note that the applied voltage applied between the injecting electron reservoirs is contained within the varying chemical potential μ_k inside the structure, depending upon the direction of the incident wave propagation (i.e., $k > 0$ or $k < 0$). The discrete sum over k reflects the finite spatial extent of the system necessary for numerical reasons. (Care must be taken to chose the corresponding energy spacing $\Delta\varepsilon(\Delta k)$ small compared to k_BT.) Additional de-phasing effects inside the open dot structure have been neglected in this model, which is adequate for experimental situations where the corresponding phase-coherence length is larger than typical classical paths through the sample.

If N_k denotes the total number of k points and N_n the number of lateral modes, the Fock space will become $2^{2N_kN_n}$ dimensional. The continuum limit then corresponds to $N_k \to \infty$.

Furthermore, we must ensure that the total interaction sum

$$V_{tot} = \tfrac{1}{2} \sum_{(nk\sigma)\neq(n'k'\sigma')} V_{(nk\sigma)(n'k'\sigma')}, \tag{2}$$

scales with N_k in the same manner as the single-particle term in the Hamiltonian (which is simply proportional to N_k). This can be accomplished by introducing a scaling factor in $V_{(nk\sigma)(n'k'\sigma')}$, reflecting the required invariance under this 'size transformation' of the system. This implies that the total interaction energy per state $V_{tot}^{state} = V_{tot}/(2N_kN_n)$ converges for $N_k \to \infty$. For the interaction matrix element, we employ the following model expression in the vicinity of a resonance E_0 (where ε_{nk} is the spin-independent part of $\varepsilon_{nk\sigma}$):

$$V_{(nk\sigma)(n'k'\sigma')} = \frac{1}{2N_kN_n}(U_{nn'} - \delta_{\sigma\sigma'}U_{nn'}^{exch}) \cos^2\left(\pi\frac{\varepsilon_{nk}-E_0}{2\Gamma}\right)\cos^2\left(\pi\frac{\varepsilon_{n'k'}-E_0}{2\Gamma}\right), \tag{3}$$

for

$$\left|\frac{\varepsilon_{nk}-E_0}{\Gamma}\right| \leqslant 1 \qquad \text{and} \qquad \left|\frac{\varepsilon_{n'k'}-E_0}{\Gamma}\right| \leqslant 1, \tag{4}$$

and zero otherwise, with U and U^{exch} the Hartree and exchange terms ($U \geqslant U^{exch} \geqslant 0$), respectively. This implies that $V_{tot}^{state} \propto U - 0.5U^{exch}$. Here, 2Γ is the total width of the interaction resonance. (This corresponds to the lifetime of the resonantly trapped charge. A Lorentzian would be a natural choice for the single-particle charge peak [3, 4] but the $\cos^2$ eliminates cut-off problems at the interaction tails in the numerical implementation.) One can see that, in contrast to the Anderson model with off-diagonal hopping terms, this many-body problem is diagonal at the cost of a continuum ($N_k \to \infty$) of interacting single-particle base states. Since the underlying Hamiltonian of the presented model includes major parts of the electron–electron interaction among all involved electronic states (propagating through the dot and resonantly enhanced at certain energies) in a full many-body formulation, this inherently accounts for screening effects (among these states) resulting from the given Coulomb matrix. (On the other hand, one must also think of the model Coulomb matrix as an effective interaction term including all further many-body screening effects due to the environment, and other continuous states not included in the model. In this case, one has to employ a screened Coulomb-kernel in the Coulomb matrix integrals. In any case, we assume a resulting peaked effective interaction matrix element.)

In order to calculate transport properties of the model we consider a non-equilibrium (due to a non-uniform chemical potential) many-body density matrix describing a thermodynamical ensemble [30]:

$$\rho = \frac{1}{Z}\exp(\hat{H}), \tag{5}$$

with the partition function $Z = \mathrm{Tr}[\exp(\hat{H})]$. (Note that, for the given form of $\hat{H}$, this density matrix has the maximum entropy form for the condition of individually given $\langle c_{nk\sigma}^{+}c_{nk\sigma}\rangle$ and $\langle\hat{H}\rangle$ with Lagrange parameters μ_k and β, respectively.) Since $\hat{H}$ is a diagonal operator with respect to the given basis we only need to evaluate an exponential function of real numbers. (This is the main reason for the form chosen of the Hamiltonian. In the numerical implementation, we have employed an 'on-the-fly' renormalization algorithm to avoid a numerical over- or under-flow of the partition function.)

In the following, we will only consider single-particle observables like the current and the spin polarization, which are linear functions of occupation numbers $c_{nk\sigma}^{+}c_{nk\sigma}$. Under this

condition we can reformulate the many-body problem as an effective single-particle problem with the following normalized Hamiltonian:

$$\hat{H}_{MF} = -\beta\left[\sum_{n,k,\sigma}(\varepsilon_{nk\sigma} + w_{nk\sigma} - \mu_k)c^+_{nk\sigma}c_{nk\sigma}\right]. \tag{6}$$

Here, $w_{nk\sigma}$ denote Lagrange parameters for the condition

$$\langle c^+_{nk\sigma}c_{nk\sigma}\rangle = \langle c^+_{nk\sigma}c_{nk\sigma}\rangle_{MF}(\forall n, k, \sigma) = f_{FD}(\varepsilon_{nk\sigma} + w_{nk\sigma} - \mu_k; T), \tag{7}$$

so that the expectation values of all occupation numbers are identical for both Hamiltonians, where f_{FD} is the Fermi–Dirac function. So far, we have not made any further approximation. As an intuitive approximation for the Lagrange parameters (in the limit $N_k \to \infty$), we now want to assume that $w_{nk\sigma}$ are linear functionals of all $\langle c^+_{\dots}c_{\dots}\rangle$ with

$$w_{nk\sigma}[\langle c^+_{\dots}c_{\dots}\rangle] = \sum_{(n'k'\sigma')\neq(nk\sigma)} V_{(nk\sigma)(n'k'\sigma')}\langle c^+_{n'k'\sigma'}c_{n'k'\sigma'}\rangle, \tag{8}$$

which is nothing but the mean-field single-particle interaction potential. (Note however that $\langle\hat{H}_{MF}\rangle_{MF} \neq \langle\hat{H}\rangle$ in general due to an 'overcounting' of the total interaction. Furthermore, one has to note that we consider first order corrections due to the energetically peaked excess interaction term here, whereas the Kondo effect of a magnetic impurity within an electron gas is a correction to the mean-field Fermi liquid behaviour with a conventional Coulomb interaction term.)

4. Occupation numbers

The peaked interaction model introduces characteristic modifications to the electronic structure which will be discussed in this section. As a prototype system, we assume a linear dispersion in the vicinity of a single sharp resonance in an open dot system with only *one* lateral mode in the leads ($N_n = 1$). In all following simulations, we will employ the mean-field approximation for $N_k \geqslant 16$ and the full density-matrix calculation for smaller N_k. The limitation of the density-matrix approach to a small number of single-particle states is due to the exponentially growing Fock space dimension (e.g., for $N_k = 15$ we obtain a 1.1×10^9-dimensional Fock space). We employed a bit-mask integer representation of Fock basis states in the numerical implementation. There is a very good agreement between these two approaches for $N_k \geqslant 12$, with a deviation in the occupation numbers below 1%. Furthermore, the results converge in the limit $N_k \to \infty$ as expected from the size-scaling invariance mentioned above. All quantities in the following simulations are taken as dimensionless real numbers, in order to be able to map the results to any given experimental situation.

Figure 1 shows the typical electron filling behaviour of the peaked interaction model for a simple example. The interaction resonance is located in the centre of the k-region. One can clearly see the energetic shift of electrons in the presence of occupied states.

The shape of the occupation distribution as a function of k suggests the definition of an effective single-particle dispersion $\varepsilon^{eff}_{nk\sigma}$ and temperature $T^{eff}_{nk\sigma}$, which are functions of the chemical potentials μ_k and the real heat-bath temperature T, such that

$$\langle c^+_{nk\sigma}c_{nk\sigma}\rangle(\mu_k, T) = f_{FD}(\varepsilon^{eff}_{nk\sigma}(\mu_k, T) - \mu_k; T^{eff}_{nk\sigma}(\mu_k, T)). \tag{9}$$

However, for k values where the occupation is still Fermi–Dirac-like (which is obviously not the case in general when we have interacting electrons, but is a good approximation for $k_BT \gg V_{tot}, \Gamma$) $\varepsilon^{eff}_{nk\sigma}$ and $T^{eff}_{nk\sigma}$ become independent of μ_k. Note that the effective dispersion introduced here only visualizes modifications to the density of states at the Fermi energy as compared to the free electron case (i.e., those k-states contribute to a change in the total

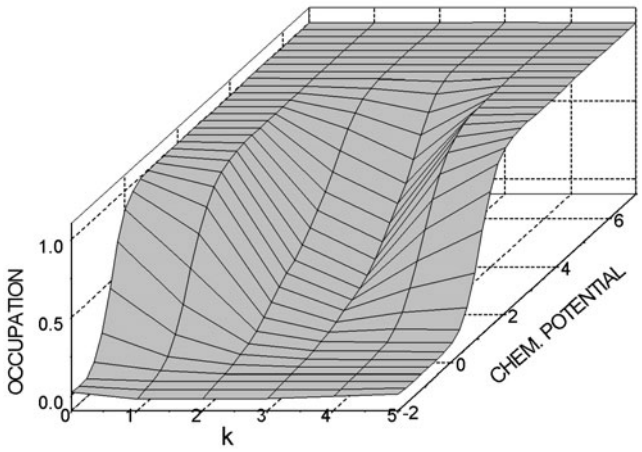

Figure 1. Occupation number $\langle c^{+}_{nk\sigma} c_{nk\sigma} \rangle$ as a function of the (common) chemical potential μ (relative to E_0) and the absolute value of the wavenumber k (relative to the interaction window) for $\Gamma = 0.4$, $U = 2.4$, $U^{exch} = 0.6U$, $k_B T = 0.2$ and $N_k = 12$ (i.e. $\approx 1.6 \times 10^7$-dimensional Fock space).

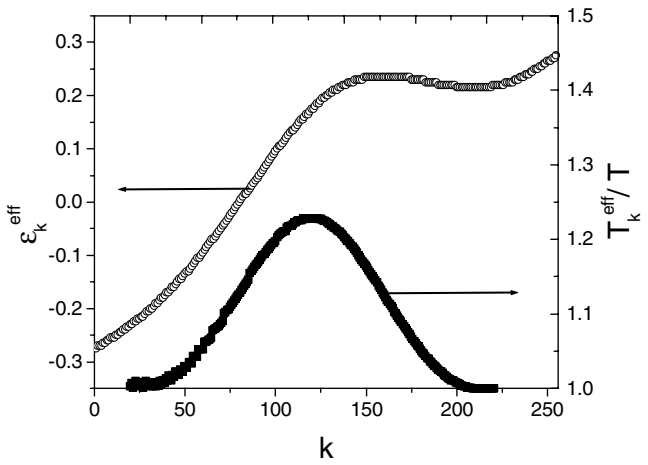

Figure 2. Effective dispersion ε^{eff}_k (relative to E_0) and effective temperature T^{eff}_k / T as a function of the absolute value of k (relative to the interaction window) for $\Gamma = 0.25$, $U = 1.0$, $U^{exch} = 0.5U$, $k_B T = 0.4$ and $N_k = 512$.

occupation for a given $\mu \pm \delta\mu$ where $\varepsilon^{eff}_{nk\sigma} \approx \mu$). Characteristic features in $\varepsilon^{eff}_{nk\sigma}$ (such as extrema) help to explain the temperature and chemical potential dependence of observables below. However, since the effective dispersion is a function of T itself we cannot expect that the temperature dependence of observables, such as the conductance, is simply given by the Fermi–Dirac broadened function at $T = 0$. In figure 2, we show a typical example of the effective dispersion and temperature. Note that the k-range shown is only a small fraction of the total k-space in the vicinity of the interaction resonance ($\varepsilon_{-k} = \varepsilon_k$ and $\varepsilon^{eff}_{-k} = \varepsilon^{eff}_k$) and that the interaction-free case corresponds to a straight line.

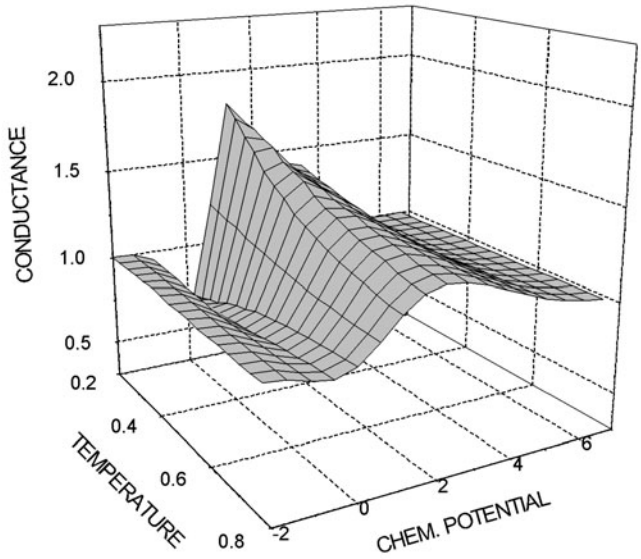

Figure 3. Normalized conductance as a function of the chemical potential μ (relative to E_0) and the temperature T for $\Gamma = 0.4$, $U = 2.4$, $U^{exch} = 0.6U$ and $N_k = 12$.

5. Conductance

The current operator $\hat{I}$ can be expressed in terms of the transmission probability $t_{nk\sigma}$ and the group velocity $v_{nk\sigma}$ (derived from $\varepsilon_{nk\sigma}$) of propagating states as

$$\hat{I} \propto \sum_{n,k,\sigma} \mathrm{sign}(k) v_{nk\sigma} t_{nk\sigma} c^{+}_{nk\sigma} c_{nk\sigma} . \tag{10}$$

Hence the linear-response conductance reads (with $\Delta\mu = \mu_{k>0} - \mu_{k<0}$)

$$G = \left. \frac{\mathrm{d}\langle \hat{I}(\Delta\mu) \rangle}{\mathrm{d}\Delta\mu} \right|_{\Delta\mu=0} . \tag{11}$$

In order to clearly identify the influence of the interaction on the conductance (entering through $c^{+}_{nk\sigma} c_{nk\sigma}$), we set the transmission probability $t_{k\sigma} = 1$ in the following examples. For realistic simulations of a given quantum dot structure, one must consider a transmission probability with a Fano resonance, which will imply further temperature dependence (due to single-particle terms).

Figure 3 illustrates the behaviour of the normalized conductance with varying temperature and chemical potential. One can clearly see an increasing effect with decreasing temperatures. Due to the repulsive interaction, the density of states at energies at the lower end of the resonance is reduced, hence the conductance is lowered (i.e., the resistance increases). This corresponds to the steeper slope in the effective dispersion which can be seen in figure 2. Once the chemical potential reaches the minimum in the effective dispersion (see figure 2) the density of states is enhanced, which is reflected in the increased conductance in figure 3. The additional peak at higher energies can be identified as the maximum of the effective dispersion (figure 2).

If we consider a Fano-type transmission probability, the interaction will modify the shape of the conductance fluctuation and its temperature dependence for $k_B T \to 0$. In the following, we will look more closely at the quantitative corrections to the conductance due to interaction effects.

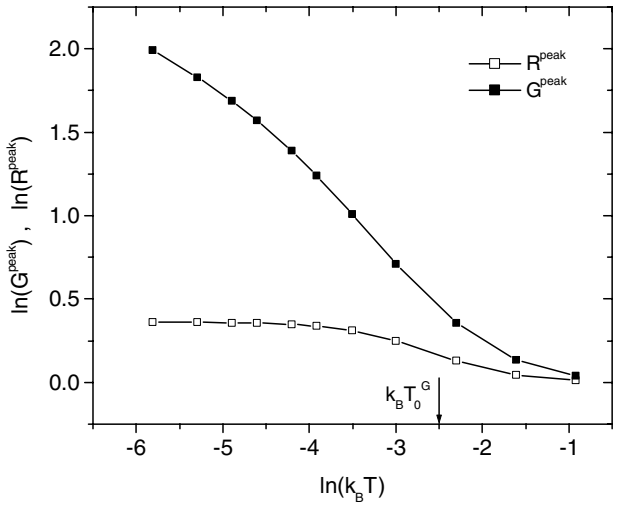

Figure 4. Peak resistance and conductance as a function of temperature. Two temperature regimes are clearly resolved ($\Gamma = 0.25$, $U = 1.0$, $U^{exch} = 0.5U$ and $N_k = 512$).

A systematic analysis of the simulated temperature dependence of the conductance modification with varying interaction energy and resonance width leads to the definition of a characteristic energy scale for the maxima in the conductance $k_B T_0^G$ and the resistance $k_B T_0^R$:

$$k_B T_0^G = \alpha^G \sqrt{\Gamma V_{tot}^{state}}, \tag{12}$$

$$k_B T_0^R = \alpha^R \sqrt{\Gamma V_{tot}^{state}}, \tag{13}$$

with fitting parameters $\alpha^G \approx 0.55$ and $\alpha^R \approx 0.31$. (One has to note that this temperature has a form reminiscent of an effective Kondo temperature [20, 21, 23]. As the peaked-interaction model has its roots in the Anderson Hamiltonian, we could expect a correspondence [31]). This characteristic energy defines two temperature regimes. Figure 4 shows the typical dependence of the conductance and resistance peaks on the temperature.

5.1. High temperatures ($T > T_0$)

In figure 5, we show the typical line shape of the conductance fluctuation as a function of the chemical potential. The parameters chosen provide $V_{tot}^{state} = 0.0846$, $k_B T_0^G = 0.0798$ and $k_B T_0^R = 0.0457$. At high temperatures, further fine structure in the conductance cannot be further resolved.

In this temperature regime, we observe a modified Boltzmann law for the scaling of the conductance and resistance peak G^{peak} and R^{peak}, respectively, as

$$G^{peak}(T) \cong G(\infty) \exp\left(\left\{\frac{T_0^G}{T}\right\}^2\right), \tag{14}$$

$$R^{peak}(T) \cong R(\infty) \exp\left(\left\{\frac{T_0^R}{T}\right\}^2\right). \tag{15}$$

Similar scaling behaviour of the conductance and resistance peaks has been observed in experimental studies of coupled open quantum dots [7, 9–11].

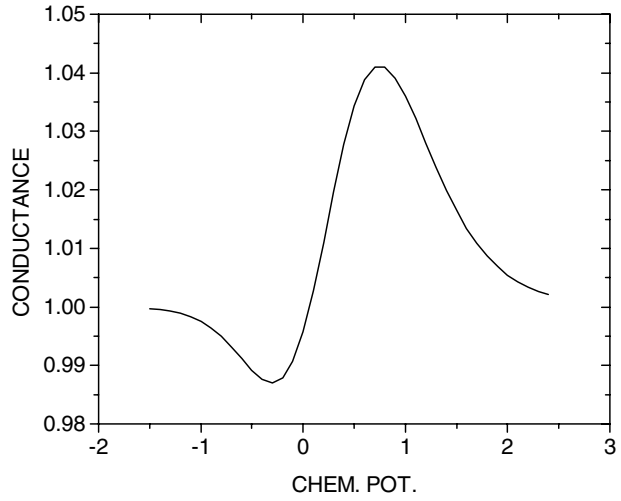

Figure 5. Normalized conductance as a function of the chemical potential μ (relative to E_0) for $k_BT = 0.4$, $\Gamma = 0.25$, $U = 1.0$, $U^{exch} = 0.5U$ and $N_k = 128$.

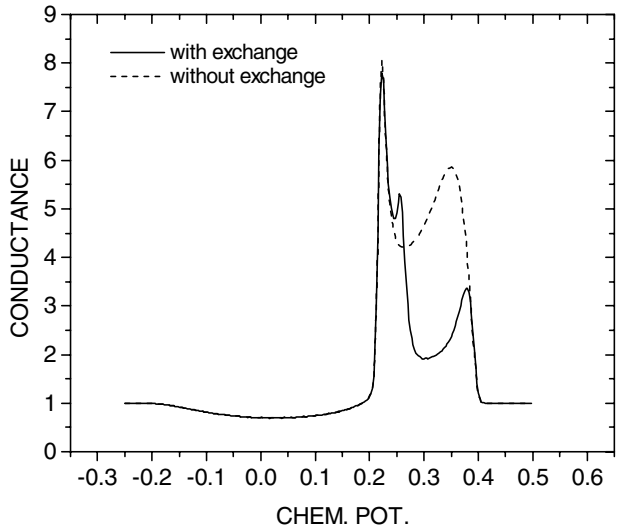

Figure 6. Normalized conductance as a function of the chemical potential μ (relative to E_0) for $k_BT = 0.0025$, $\Delta\varepsilon_{\uparrow\downarrow} = 0.002$, $\Gamma = 0.25$ and $N_k = 256$. With exchange: $U = 1.0$, $U^{exch} = 0.5U$. Without exchange: $U = 0.75$, $U^{exch} = 0$. ($V_{tot}^{state} \propto U - 0.5U^{exch}$ is constant.)

5.2. Low temperatures ($T \ll T_0$)

The line shape of the conductance fluctuation as a function of the chemical potential is shown in figure 6. V_{tot}^{state}, $k_BT_0^G$ and $k_BT_0^R$ are identical to the high temperature case. Here, we have assumed a spin splitting of $\Delta\varepsilon_{\uparrow\downarrow} = 0.002$, in order to introduce a preferred spin direction. At these temperatures, all the features of the effective dispersion relation are resolved (see figure 2). The additional small third peak stems from the exchange-lowered interaction energy for electrons with parallel spin alignment. (Note that, in this case, each spin direction σ has

a different effective dispersion, reflecting the exchange lowering.) Further exchange-induced effects will be discussed below in connection with spin polarization.

For low temperatures, there is a significantly different temperature dependence of the conductance and the resistance peak, as can be seen in figures 4 and 6. While the conductance exhibits a diverging sharply peaked fine structure for $T \to 0$, the resistance maximum saturates (similar to [15]). Simulations show that the saturation resistance can be expanded in terms of a dimensionless parameter $x \equiv V_{tot}^{state}/\Gamma$ as

$$R^{peak}(T \to 0) \cong 1 + \beta x + \mathrm{O}(x^2), \tag{16}$$

and the numerically determined coefficient $\beta \approx 1.28$ (for $x \leqslant 4$). The detailed scaling behaviour of the conductance peaks is currently under investigation. Preliminary results suggest an analogy to many-body corrections in quantum dots in the tunnelling regime [16–21]. A connection to the effective exchange energy J [31] of the Anderson model might be of some importance.

6. Spin polarization

Spin polarization in external magnetic fields gives further insight into the electronic structure of the open quantum dot system (see [22] for a comparison with the magnetic properties of an Anderson impurity). In our case, the characteristic temperature T_0 separates two different regimes in the response of the electron spins to a magnetic field. In the following we discuss the influence of the field-induced spin splitting $\Delta\varepsilon_{\uparrow\downarrow}$ due to a small external field B ($\Delta\varepsilon_{\uparrow\downarrow}(B) < k_B T$). We use a polarization S defined as

$$S = \frac{1}{2N_k N_n} \sum_{nk\sigma} \mathrm{sign}(\sigma) \langle c^{+}_{nk\sigma} c_{nk\sigma} \rangle. \tag{17}$$

6.1. High temperatures ($T \gg T_0$)

In this temperature regime we observe Pauli spin paramagnetism with

$$\chi \equiv \left.\frac{\mathrm{d}S}{\mathrm{d}B}\right|_{B=0} \propto (k_B T)^{-1}. \tag{18}$$

6.2. Low temperatures ($T \ll T_0$)

Depending on the exchange energy relative to the total interaction energy, the system can exhibit an exchange-enhanced spin polarization. The total spin polarization is plotted in figure 7 as function of the temperature for a small fixed (see above) magnetic field with varying energy (but constant V_{tot}^{state}) as a parameter.

7. Conclusions

We have presented a many-body model for the description of electron interaction effects in open quantum dot structures based on the Anderson Hamiltonian. The influence of energetically peaked interaction terms on the conductance has been discussed as a function of the temperature. The identification of characteristic temperature introduces an energy scale to the system, separating different temperature regimes. Quantitative expressions for the temperature dependence of interaction-introduced conductance fluctuations have been derived.

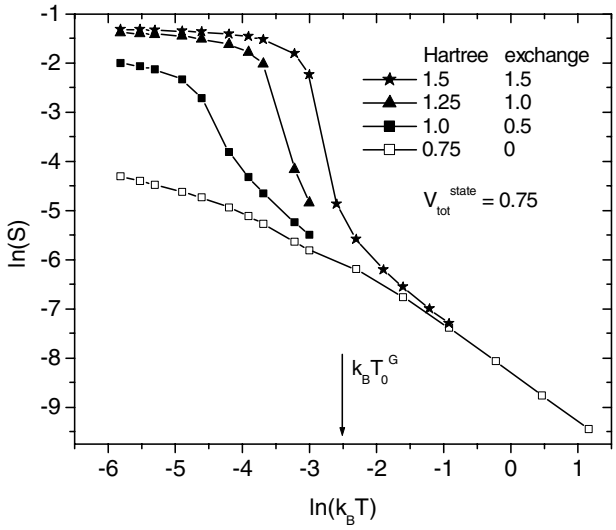

Figure 7. Total spin polarization S as a function of temperature T for $\Delta\varepsilon_{\uparrow\downarrow} = 0.002$, $\Gamma = 0.25$ and $N_k = 512$. ($V_{tot}^{state} \propto U - 0.5U^{exch}$ is constant.)

A detailed comparison of experimental results with the predictions obtained from the peaked-interaction model can be found in [32].

The extension of the model, with the inclusion of Fano resonances in the single-particle transmission probability, is straightforward. Further investigations will discuss the role of spin–orbit coupling terms and the significance of correlation terms in the interaction Hamiltonian. Details of the conductance peak fine structure and the temperature dependence for $T \approx T_0$ and $T \to 0$ remain to be clarified.

Acknowledgments

The authors acknowledge helpful discussions with I Knezevic. Our work was supported by the Office of Naval Research and the Alexander von Humboldt foundation (Feodor Lynen program).

References

[1] Akis R, Ferry D K and Bird J P 1996 *Phys. Rev.* B **54** 17705
[2] Bird J P, Akis R, Ferry D K, Vasileska D, Cooper J, Aoyagi Y and Sugano T 1999 *Phys. Rev. Lett.* **82** 4691
[3] Akis R, Bird J P, Ferry D K and Vasileska D 2000 *Physica* E **7** 745
[4] Akis R, Bird J P and Ferry D K 2002 *Appl. Phys. Lett.* **81** 129
[5] Heller E J 1984 *Phys. Rev. Lett.* **53** 1515
[6] de Moura A P, Lai Y C, Akis R, Bird J P and Ferry D K 2002 *Phys. Rev. Lett.* **88** 236804
[7] Shailos A, Prasad C, Elhassan M, Akis R, Ferry D K, Bird J P, Aoki N, Lin L H, Ochiai Y, Ishibashi K and Aoyagi Y 2001 *Phys. Rev.* B **64** 193302
[8] Bird J P, Shailos A, Elhassan M, Prasad C, Ferry D K, Lin L H, Aoki N, Ochiai Y and Aoyagi Y 2000 *Nanotechnology* **11** 365
[9] Ge F, Prasad C, Andresen A, Bird J P, Ferry D K, Lin L H, Aoki N, Nakao K, Ochiai Y, Ishibashi K, Aoyagi Y and Sugano T 2000 *Ann. Phys., Lpz.* **9** 65
[10] Andresen A, Prasad C, Ge F, Lin L H, Aoki N, Nakao N, Bird J P, Ferry D K, Ochiai Y, Ishibashi K, Aoyagi Y and Sugano T *Phys. Rev.* B **60** 16050

[11] Lin L H, Aoki N, Nakao K, Andresen A, Prasad C, Ge F, Bird J P, Ferry D K, Ochiai Y, Ishibashi K, Aoyagi Y and Sugano T 1999 *Phys. Rev.* B **60** 16299
[12] Usuki T, Saito M, Takatsu M, Kiehl R A and Yokoyama N 1995 *Phys. Rev.* B **52** 8244
[13] Shailos A, Bird J P, Prasad C, Elhassan M, Shifren L, Ferry D K, Lin L H, Aoki N, Ochiai Y, Ishibashi K and Aoyagi Y 2001 *Phys. Rev.* B **63** 241302
[14] Abrahams E 1999 *Ann. Phys., Lpz.* **8** 539
[15] Kondo J 1964 *Prog. Theor. Phys. (Kyoto)* **32** 37
[16] Ng T K and Lee P A 1988 *Phys. Rev. Lett.* **61** 1768
[17] Meir Y, Wingreen N S and Lee P A 1991 *Phys. Rev. Lett.* **66** 3048
[18] Meir Y, Wingreen N S and Lee P A 1993 *Phys. Rev. Lett.* **70** 2601
[19] Wingreen N S and Meir Y 1994 *Phys. Rev.* B **49** 11040
[20] Goldhaber-Gordon D, Göres J, Kastner M A, Shtrikman H, Mahalu D and Meirav U 1998 *Phys. Rev. Lett.* **81** 5225
[21] Van der Wiel W G, De Franceschi S, Fujisawa T, Elzerman J M, Tarucha S and Kouwenhoven L P 2000 *Science* **289** 2105
[22] Anderson P W 1961 *Phys. Rev.* **124** 41
[23] Úsághy O, Kroha J, Szunyogh L and Zawadowski A 2000 *Phys. Rev. Lett.* **85** 2557
[24] Ferry D K and Goodnick S M 1997 *Transport in Nanostructures* (Cambridge: Cambridge University Press)
[25] Akis R, Ferry D K and Bird J P 1997 *Phys. Rev. Lett.* **79** 123
[26] Bird J P, Akis R and Ferry D K 1999 *Phys. Rev.* B **60** 13676
[27] Zozoulenko I V, Schuster R, Gerggren K F and Ensslin K 1997 *Phys. Rev.* B **55** R10209
[28] Zozoulenko I V and Berggren K F 1997 *Phys. Rev.* B **56** 6931
[29] Fano U 1961 *Phys. Rev.* **124** 1866
[30] Indlekofer K M and Lüth H 2000 *Phys. Rev.* B **62** 13016
[31] Schrieffer J R and Wolf P A 1966 *Phys. Rev.* **149** 491
[32] Indlekofer K M, Bird J P, Akis R, Ferry D K and Goodnick S M 2002 *Appl. Phys. Lett.* **81** 3861